Geomorphology 287 (2017) 116–125

Contents lists available at ScienceDirect

Geomorphology

journal homepage: www.elsevier.com/locate/geomorph

Temporal dynamics of suspended sediment transport in a glacierized Andean basin

Luca Mao *, Ricardo Carrillo

Pontificia Universidad Católica de Chile, Department of Ecosystems and Environments, Santiago, Chile

ARTICLE INFO

Article history:
Received 19 August 2015
Received in revised form 29 January 2016
Accepted 3 February 2016
Available online 5 February 2016

Keywords:
Suspended sediment transport
Hysteresis
Glacier melting
Chile

ABSTRACT

Suspended sediment transport can affect water quality and aquatic ecosystems, and its quantification is of the highest importance for river and watershed management. Suspended sediment concentration (SSC) and discharge were measured at two locations in the Estero Morales, a Chilean Andean stream draining a small basin (27 km^2) hosting glacierized areas of about 1.8 km^2. Approximately half of the suspended sediment yield (470 t $year^{-1}$ km^{-2}) was transported during the snowmelt period and half during glacier melting. The hysteresis patterns between discharge and SSC were calculated for each daily hydrograph and were analysed to shed light on the location and activity of different sediment sources at the basin scale. During snowmelt, an unlimited supply of fine sediments is provided in the lower and middle part of the basin and hysteresis patterns tend to be clockwise as the peaks in SSC precede the peak of discharge in daily hydrographs. Instead, during glacier melting the source of fine sediments is the proglacial area, producing counterclockwise hysteresis. It is suggested that the analysis of hysteretic patterns over time provides a simple concept for interpreting variability of location and activity of sediment sources at the basin scale.

1. Introduction

The quantification of suspended sediment transport in river systems is of the highest importance for ecologists and for land- and water-use managers. Sediments in suspension convey nutrient and contaminant loading that can affect aquatic ecosystems (e.g. Wood and Armitage, 1999; Bilotta and Brazier, 2008) and water quality for human consumption (e.g. Ryan, 1991). Also, fine sediments can infiltrate gravel affecting fish and macroinvertebrates (e.g. Wilber and Clarke, 2001; Blettler et al., 2015) and increasing coarse sediment transport (Curran and Wilcock, 2005). Fine sediments transported in suspension can be recruited from the river network (bed and bank erosion) or can be sourced by the basin, especially due to soil erosion, gully erosion, and mass failure such as landslides or debris flows. Beside the natural sources of fine sediments, human activities such as overgrazing, agriculture, forest and mining operations, and urbanization can remarkably increase the availability of sediments (e.g. Owens et al., 2005). Sediment sources can be investigated using radionuclides as fingerprinting techniques (Haddadchi et al., 2013) which permit the quantification of the relative contributions of various sources to the total yield (e.g. Walling et al., 2006; Collins et al., 2013). Also, the source of fine sediments transported in suspension may be explored by measuring the colour of sediments using diffuse reflectance spectrometry (Martínez-Carreras et al., 2010), the geochemical properties of sediments (Motha et al., 2003), or the size of sediments (Walling and Amos, 1999; Davis and Fox, 2009). Alternatively, sources and degree of activity of sediment sources can be inferred by analysing the changes in the suspended sediment concentration (SSC) with respect to the changes in liquid discharge (Q) at the scale of a single event. If the SSC-Q relationship is scattered and non-unique, hysteretic loops can often be detected and classified as clockwise (when the peak of SSC peak occurs before the peak of Q) or counterclockwise loop (opposite behaviour) (e.g. Williams, 1989; Lenzi and Marchi, 2000; Gao and Josefson, 2012; Yeshaneh et al., 2013).

Clockwise hysteresis has been attributed to unlimited sediment supply. At the scale of the single flood event, clockwise hysteresis can be due to early exhaustion of sediment sources, nearby sources of sediments, and sediment being provided by the channel bed rather than the slopes (e.g. Asselman, 1999; Rovira and Batalla, 2006; Gao and Pasternack, 2007). Conversely, counterclockwise hysteresis may be due to the fact that the sediment source is far from the point of monitoring (Klein, 1984), bank failures which tend to occur after the peak of the flood when the bank is saturated (Rinaldi et al., 2004), and sediment depletion in the channel system (Walling and Webb, 1982). In an attempt to explore quantitatively the degree of the hysteretic loops, Aich et al. (2014) proposed a dimensionless metric for an hysteresis index that is provided by the size of the loop and its direction. By using normalized values of SSC and Q, the resulting index is comparable between events and sites, improving previously proposed indices (e.g. Langlois et al., 2005; Lawler et al., 2006).

Apart from the evaluation of sediment availability at the scale of a single flood event, hysteresis has been used to explore sediment dynamics over longer terms. Analysing the dynamics of suspended sediment in the Rhine River, Asselman (1999) reported a decrease of

* Corresponding author at: Department of Ecosystems and Environments, Pontificia Universidad Católica de Chile, Av. Vicuña Mackenna 4860, Macul, Santiago, Chile.
E-mail address: lmao@uc.cl (L. Mao).

http://dx.doi.org/10.1016/j.geomorph.2016.02.003
0169-555X/

sediment concentration from winter to spring and a dominance of clockwise hysteresis during early floods, and related this to a progressive sediment depletion during a hydrological year. This depletion effect through time was also found by analysing hysteretic patterns of single floods in a 300 km^2 basin of central New York (Gao and Josefson, 2012). They reported that clockwise loops are more frequent during snowmelt, due to the ready-availability of in-channel fine sediments, and to the fact that higher elevations covered by snow do not contribute to sediment generation. Analysing rainfall-generated floods on three small basins in Mexico, Duvert et al. (2010) also reported strong seasonality in suspended sediment transport, due to the filling and depletion of in-channel sediment storage, and connectivity of sediment sources at the basin scale. Fan et al. (2013) explicitly mention a "store-release" set of processes at the seasonal scale, stating that sediments are being prepared in winter and spring (when counterclockwise hysteresis are more common), and exported in rainy seasons.

In basins dominated by snowmelt, evidence from the literature is similar, and the relationship between hysteresis and sediment sources is even more closely related to seasonality. For example, Iida et al. (2012) showed that early snowmelt events featured clockwise hysteresis due to the flushing of sediments stored on the channel bed, whereas during the late snowmelt season, counterclockwise loops were more common due to the dominance of sediment sources at the basin scale. On glacierized basins, hysteresis loops can be observed every day due to the typical diurnal variation of discharge and suspended sediments, but field evidence is scarce. Singh et al. (2005) analysed daily fluctuations of discharge due to the ablation of a large Himalayan glacier reporting clockwise hysteresis for all the ablation season. On the other hand, Wulf et al. (2012) showed that in the western Himalaya more suspended sediment is transported during late summer than during the onset of the monsoon season, implying that transiently stored material is not mobilized with the first flood events. However, Stott et al. (2014) registered both clockwise and anticlockwise hysteresis in small glacierized basins in south-west Greenland. Despite this growing body of research on suspended sediment dynamics in glacierized basins, virtually no evidence is available from the Southern Andean Range, where glaciers are shrinking (Rivera et al., 2000; Masiokas et al., 2009; Pellicciotti et al., 2014) and water supplied by glacier-melting is crucial for agriculture, hydropower generation, and drinking water supplies. In this paper we aim to explore the temporal dynamics of SSC in a small glacierized basin in the southern Andes. Suspended sediment concentration and yield, and hysteresis associated with daily fluctuations of discharges during the snow and glacier melt periods of two seasons are used to illustrate changes and dynamics of sediment availability at the basin scale.

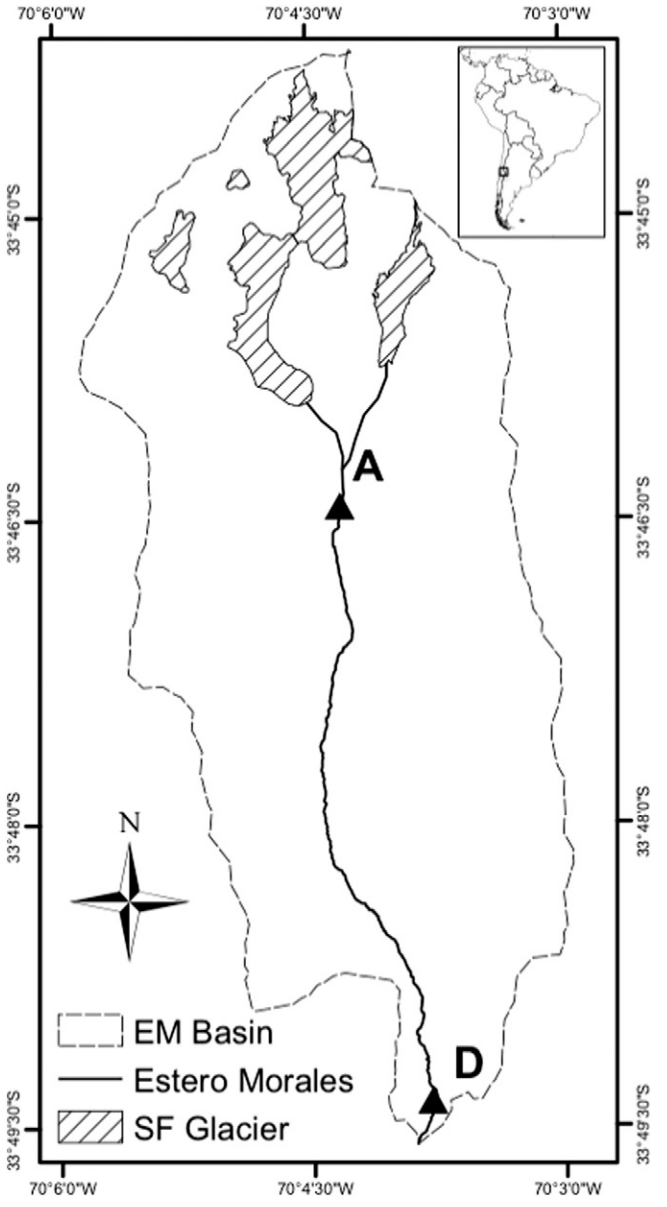

Fig. 1. Map of the Estero Morales, showing the location of the monitoring sites D and A.

2. Materials and methods

The study has been carried out in the Estero Morales, a high-gradient stream of the Southern Andes located in the Chilean Metropolitan Region, approximately 100 km southeast from Santiago (Fig. 1). The basin ranges from 1850 to 3815 m a.s.l., and extends for 27 km^2. It drains into the Maipo basin, which eventually flows to the Pacific Ocean. In its upper part (at elevations higher than 2690 m a.s.l.), the basin hosts glacierized areas, some uncovered and some covered by debris (Fig. 2). The biggest portion of the glacier is called San Francisco, and overall the glacierized area has a current extent of 1.8 km^2 (Fig. 1). Although glaciological studies on this basin are still not available, recent evidence from the surrounding area shows that glaciers are retreating at a considerable rate. For example, the Juncal Sur glacier in the upper part of the Río Maipo basin has retreated approximately 50 m year^{-1} and has thinned at a rate of 1 m year^{-1} from 1955 to 1997 (Rivera et al., 2000; Masiokas et al., 2009). The mean annual rainfall measured in the nearest station (Embalse El Yeso station, installed at 2475 m a.s.l.) is around 574 mm, and precipitation occurs mainly as snowfall from May to September (approximately 82% of total precipitation), with occasional summer convective storms. Runoff is dominated by snowmelt in late spring (from late September to November), and glacier melt from December to March, providing a long season of daily fluctuations of discharge (Fig. 3).

The solid geology of the basin consists of limestones and conglomerate breccias, with some volcanic formations on the eastern slopes (Infante Fabres, 2009). Fluvial and glacial Quaternary deposits are very common, and alluvial fans, moraine deposits and talus slopes are widespread features of the landscape (Fig. 2). When present, soils are very thin and covered by montane grassland with dispersed shrubs dominated by *Chuquiraga oppositifolia* and *Molinum spinosum*. The average slope of the main channel is about 0.105 m m^{-1}. However, three segments with different morphology could be recognised. From the glacier to the end of a moraine that confined the channel down to 2442 m a.s.l., the channel is steep (0.15 m m^{-1}) and featuring cascade and step-pool reaches (sensu Montgomery and Buffington, 1997). From 2442 to 2238 m a.s.l. the stream flows in the relatively large U-shape "hanging" valley with riffle-pool morphology, with large coarse bars and multiple channels on some reaches (Fig. 2). From 2238 m a.s.l. to the confluence

Fig. 2. Upstream view of the Estero Morales valley (on the left) and view of the lower portion of the glacierized area (on the right).

with the El Volcan River, the river cuts into glacier deposits. In this lower portion which is very confined and steep (0.14 m m^{-1}), the stream is characterized by coarse sediments and a cascade/step-pool morphology.

Two monitoring sites were established on the Estero Morales (Fig. 1), namely D near the confluence with El Volcan River (drainage area 26.70 km^2; 6.96% of the basin covered by glacierized areas, 26 km^2 7.15% at D), and A (drainage area 10.92 km^2; 17.03% of the basin covered by glacierized areas). In July 2013, a multiparameter water quality sonde (OTT Hydrolab MS5) was installed on D, measuring pH, water temperature, electrical conductivity and turbidity within a range from 0 to 3000 NTU (± 1% up to 100 NTU; ± 3% from 100 to 400 NTU; ± 5% from 400 to 3000 NTU). Water stage was monitored in D using a pressure transducer sensor in a cross-section confined by the presence of a bridge. Turbidity and water stage were monitored at the instrumented cross-section D at 1 h resolution until October 2014 and then at 10 min resolution from October 2014 to April 2015. Rainfall was measured in D every 5 min by a non-heated tipping-bucket rain gauge. A natural cross-section located at A (see Fig. 1) was instrumented in February 2014 with similar equipment previously installed in D, in order to monitor water stage, temperature, conductivity and turbidity at 10 minute resolution.

Stage-discharge rating curves were established for both D and A based on 32 and 18 discharge measurements, respectively. Discharge was measured using the salt dilution method (Moore, 2005) for a range of field conditions ranging from 0.11 to 2.56 m^3 s^{-1}.

In order to establish an empirical relationship between NTU and the concentration of sediments in suspension (SSC, in mg l^{-1}), water samples were collected using a USGS DH-48 handheld depth integrated water sampler. Samples were collected only randomly in D during the 2013–2014 season. Conversely, from December 2014 to March 2015, samples were collected once a month at 3 hourly spaced intervals during 24 h, in order to take samples during a wide range of discharges (0.8–2.3 m^3 s^{-1}) and NTU (8–2424). Overall, 55 and 36 samples were collected in D and A, respectively. The collected samples were filtered in order to assess the concentration of suspended sediments in g l^{-1}. The power-law empirical regressions between NTU and SSC for both D and A sites were fitted with coefficients of determination of 0.874 and 0.862, respectively.

At the daily scale, fluctuations of discharge and associated suspended sediment transport exhibited a certain degree of hysteresis, which was quantitatively assessed using metrics recently proposed in literature (Langlois et al., 2005; Lawler et al., 2006; Aich et al., 2014). The hysteresis index (H) proposed by Langlois et al. (2005) relates the area under the Q-SSC curves obtained for the rising and falling limb of hydrographs. Hysteresis is classified as clockwise when $H > 1$ (SSC peaks before Q), and counterclockwise when $H < 1$ (SSC peaks after Q). Lawler et al. (2006) developed a dimensionless hysteresis index (MI_{mid}) that is calculated comparing the value of SSC measured during the rising and the falling limb of the hydrograph at a discharge (Q_{mid}) calculated as the average between the minimum and maximum discharge of the daily fluctuation. When the SSC is higher in the rising limb of the hydrograph (indicating clockwise hysteresis), the HI_{mid} is higher than 0. On the other hand, $HI_{mid} < 0$ indicates a counterclockwise hysteresis. Also, the higher the deviation from 0, the greater the hysteretic loop. Because the value of this index depends on the absolute values of measured variables (SSC and Q), Aich et al. (2014) proposed the use of normalized discharge and SSC (values then range from 0 to 1). Rising and falling limbs of the hydrograph are separated by a line starting at the Q_{max} and ending at the last value of the temporal series. Then, the distance from this line to the farther value of SSC on the rising and falling limb are calculated and totalled. The calculated hysteresis index (HI) is positive if the loop is clockwise, and negative if the loop is counterclockwise.

Fig. 3. Example of daily fluctuations of discharge at the section D of the Estero Morales due to glacier melting. The photos were taken on 14th January 2015 at 10:00 (on the left) and 20:00 (on the right).

3. Results

3.1. Relationships between discharge and suspended sediment concentration

Relationships between paired measurements of liquid discharge and suspended sediment concentration have been obtained as in similar studies. Fig. 4 shows an example of the very wide scatter that exists in the relationship between the two variables. For instance, at a discharge of 2 $m^3 s^{-1}$, in the monitoring site D suspended sediment concentrations ranging from 63 to 903 mg l^{-1} were registered during the 2013–2014 season. Besides, a concentration of 400 mg l^{-1} was registered during flow conditions ranging from 1.6 to 3.4 $m^3 s^{-1}$ (Fig. 4). Due to this very wide scatter in the data, the coefficient of determination of a power law regression is very poor ($R^2 = 0.343$ for D in 2013–2014; $R^2 = 0.306$ for D in 2014–2015; $R^2 = 0.465$ for A in 2014–2015). The coefficients of determination of the regressions between Q and SSC increase substantially if data are analysed at the monthly scale. Table 1 shows that the correlations between SSC and Q are weaker for the first months of the snowmelt season, and are generally stronger when glacier melt becomes the most important source of water discharge (i.e. from December). Also, Fig. 4 shows that regression lines plot differently depending on the months from which they are derived, shifting towards the right as the summer season progresses, suggesting that sediments are progressively less available from spring to summer season. For example, for transporting 200 mg l^{-1} of sediments in suspension, 1.27 $m^3 s^{-1}$ is needed in October 2013, 1.69 $m^3 s^{-1}$ in December 2013, and up to 2.68 $m^3 s^{-1}$ in February 2014. A *F-test* ($p < 0.05$) conducted on Q and SSC data collected in 2013–2014 in D (Fig. 4) shows that October is statistically different than November (p-value = 1.4E−8) and that December is significantly different than January (p-value = 0.0012), whereas for the other paired months the p-value is always higher than 0.3. This suggests that suspended sediment transport generated by diverse runoff-generating processes is significantly different. In fact, the data collected from January to March, characterized by pure glacier melting, are not significantly different. Very similar results are available for data collected in 2014–2015.

3.2. Suspended sediment yield (SSY)

Paired values of discharge and suspended sediment concentration were used to calculate SSY at the monthly scale for the two study years. Because no suspended sediment could be measured at significant concentration after March and before October, sediment yield is virtually limited to 6 months. Fig. 5 shows that suspended sediment yield in October and November ranges from 50 to 70 t per month per km^2 in the monitoring site D. Runoff in October and November is mostly due to snowmelt as rainfall is very unusual and a significant percentage of the basin is still covered by snow. Fig. 5 shows the percentage of the basin covered by snow at the end of each month, as calculated using satellite images. At the beginning of October 2013 and 2014, nearly 80% of the basin upstream of the monitoring site D was covered by snow, and this percentage reduced to approximately 50% by the end of October, and then 20% by the end of November. December therefore is a month in which glacier melting becomes important as a source of runoff generation, and by the middle of December virtually all liquid discharges are produced by the glacier melting. Sediment yield during the central summer months (December and January) is higher than 50 t per month per km^2 in D, and during the 2013–2014 monitoring period was even higher than 100 t per month per km^2. After that, suspended sediment yield reduces to approximately 50 t per month per km^2 in February and March. The dynamics of sediment yield over time is relatively similar for the two monitoring seasons at site D, even if sediment yield is higher in summertime in 2013–2014, possibly due to different availability of sediments at the basin scale, which could not be assessed in this study. Information from monitoring site A is more scattered and difficult to interpret as no data are available for January 2014–2015 (Fig. 5). However, the amount of transported fine sediments appears higher than in D, and sediment yield in late summer time was lower than in November and December as in D. The overall amount of sediments transported in suspension out of the basin at site D is approximately 470 t $year^{-1}$ km^{-2}, , 51% of which was due to snowmelt, 47% due to glacier melting, and approximately only 2% due to rainfall events. This figure is relatively similar if calculated for monitoring site A, being the fine sediment yield of 430 t $year^{-1}$ km^{-2}, and the percentage of it occurring in snowmelt, glacier melting, and rainfall events being around 57, 41, and 2%, respectively.

3.3. Hysteresis of suspended sediment transport

Daily fluctuations of discharge due to snow and glacier melting show some degree of hysteresis with the concentration of suspended sediments. Fig. 6 shows two daily hydrographs which occurred in December 2013 and January 2104, which were similar in terms of duration and magnitude, but featured two different hysteresis patterns. In fact, every daily hydrograph features some degree of hysteresis, which was quantified using the three indices (Langlois et al., 2005; Lawler et al., 2006; Aich et al., 2014). Because each index is calculated taking into account different characteristics of the rising and falling limbs of Q and SSC, they can provide different values for the same event, and are not

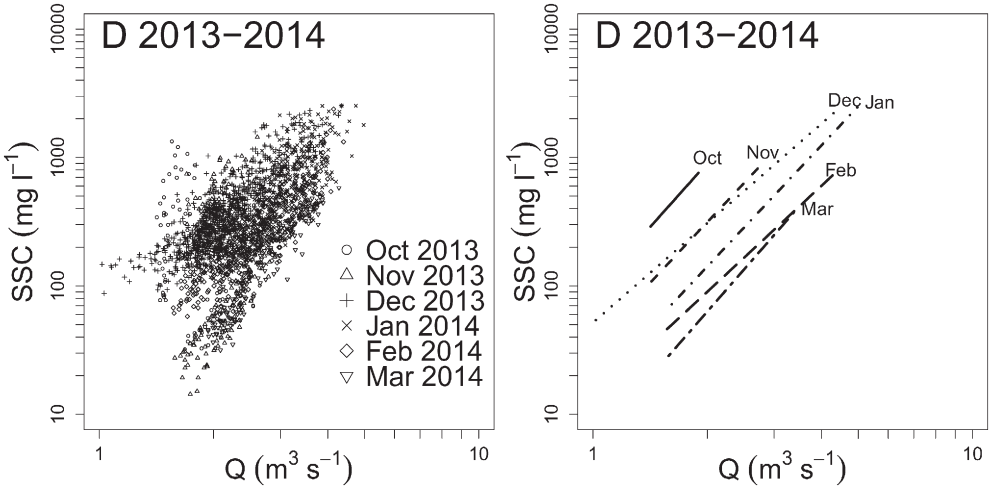

Fig. 4. Relationship between discharge and suspended sediment concentration. Data collected on the monitoring point D on the 2013–2014 season's is showed (on the left) along with the best-fit power-law regressions (on the right), which are reported on Table 1.

Table 1
Coefficients (a), exponents (b), standard errors (Se.), coefficients of determination, number of data available, and p-values for the power law regressions relating suspended sediment transport (mg l^{-1}) and liquid discharge (m^3 s^{-1}) for data collected on spring and summer months of the two seasons (2013–2014 and 2014–2015).

Season	Site	Month	a	b	Se. a	Se. b	n	R^2	p
2013–2014	D	Oct	1.171	6.827	0.282	1.456	49	0.319	2.39E−05
		Nov	1.567	2.976	0.069	0.231	273	0.380	<2.2E−16
		Dec	1.878	2.076	0.020	0.056	744	0.651	<2.2E−16
		Jan	1.300	2.841	0.033	0.073	689	0.688	<2.2E−16
		Feb	1.152	2.611	0.043	0.105	308	0.669	<2.2E−16
		Mar	0.528	3.906	0.071	0.205	159	0.698	<2.2E−16
2014–2015	D	Oct	0.718	4.543	0.090	0.226	739	0.353	<2.2E−16
		Nov	0.619	4.241	0.033	0.079	3219	0.472	<2.2E−16
		Dec	1.492	3.187	0.017	0.052	3209	0.541	<2.2E−16
		Jan	1.624	3.172	0.019	0.061	2737	0.496	<2.2E−16
		Feb	0.343	6.017	0.026	0.084	3484	0.595	<2.2E−16
		Mar	0.264	6.597	0.030	0.105	3529	0.527	<2.2E−16
	A	Oct							
		Nov	1.834	2.667	0.023	0.085	1800	0.353	<2.2E−16
		Dec	2.441	0.883	0.006	0.038	2719	0.167	<2.2E−16
		Jan	2.006	3.438	0.008	0.059	1903	0.642	<2.2E−16
		Feb							
		Mar	2.316	2.573	0.004	0.025	3475	0.752	<2.2E−16

directly comparable among them. For instance, the flood that occurred on the 26th–27th December 2013 featured clockwise hysteresis, which was quantified as 0.28, 1.96, and 0.53 using the Aich et al. (2014); Langlois et al. (2005), and the Lawler et al. (2006) approaches, respectively (Fig. 6). Being the only parameter calculated on normalized values of Q and SSC, the recent Aich's HI index is the only one which can be used to assess the absolute degree of hysteresis, as values can range from −1.41 to 1.41. Following Aich's HI index, the 26th–27th December 2013 would therefore result being only slightly clockwise (Fig. 6).

Fig. 7 shows the range of hysteresis indices obtained for each daily hydrograph, grouped at the monthly scale for the sake of clarity as for the relationships between discharge and suspended sediment concentration. Although these indices measure hysteresis in different ways, some general trends are recognisable. Overall, in monitoring site D, hydrographs of the very early snow melt (October) tend to feature very limited hysteresis, thus suggesting that the relationship between Q and SSC at the flood scale tend to be less scattered. As the snowmelt season progresses, the hysteresis at the flood scale tend to become clockwise, suggesting that the sources of fine sediments are ready-available. Hysteresis tend to be clockwise in November for both monitoring years, but also in December in 2014–2015 probably due to higher snow accumulation during the winter time. Next, when glacier melt becomes the dominant source of runoff, hysteresis tends to be preferentially counterclockwise, as all indices become progressively lower. By February, when daily fluctuations of discharge due to glacier melt are smoother and the magnitude of flood peaks reduces, hysteresis is predominantly counterclockwise, thus suggesting limited sediment supply conditions. At the very end of the glacier melt period, all indices tend to increase. This could be related to the occurrence of floods generated by rainfall events, which tend to happen in March, before precipitation will occur as snowfall from April.

Evidence of hysteresis for glacier melt events registered in A is less straightforward to read because of the lack of data in January 2015, but a tendency for hysteresis to be progressively clockwise at the beginning of the melt season and then progressively counterclockwise towards the end of the season is evident (Fig. 7).

3.4. Celerity of discharge and suspended sediment concentration along the main channel

Because discharge and suspended sediment concentration were measured in both A and D at the same time in 2014–2015, daily fluctuations of these two variables can be compared in order to assess the celerity of Q and SSC from A to D. Since multiple or asymmetric peaks

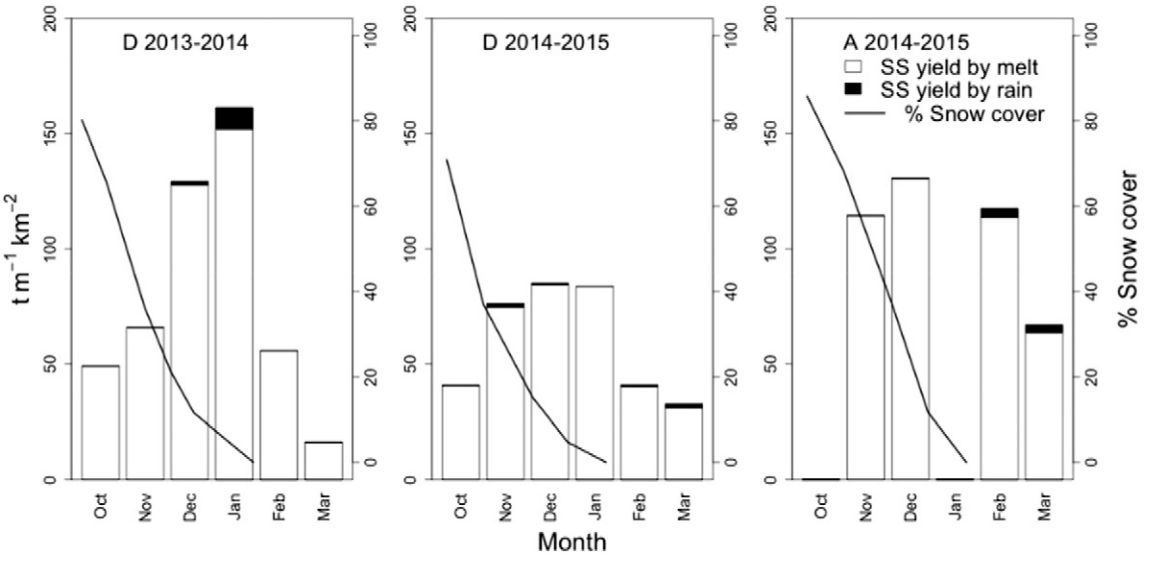

Fig. 5. Monthly sediment yield and percentage of snow cover at the end of each month for the monitoring sites A and D.

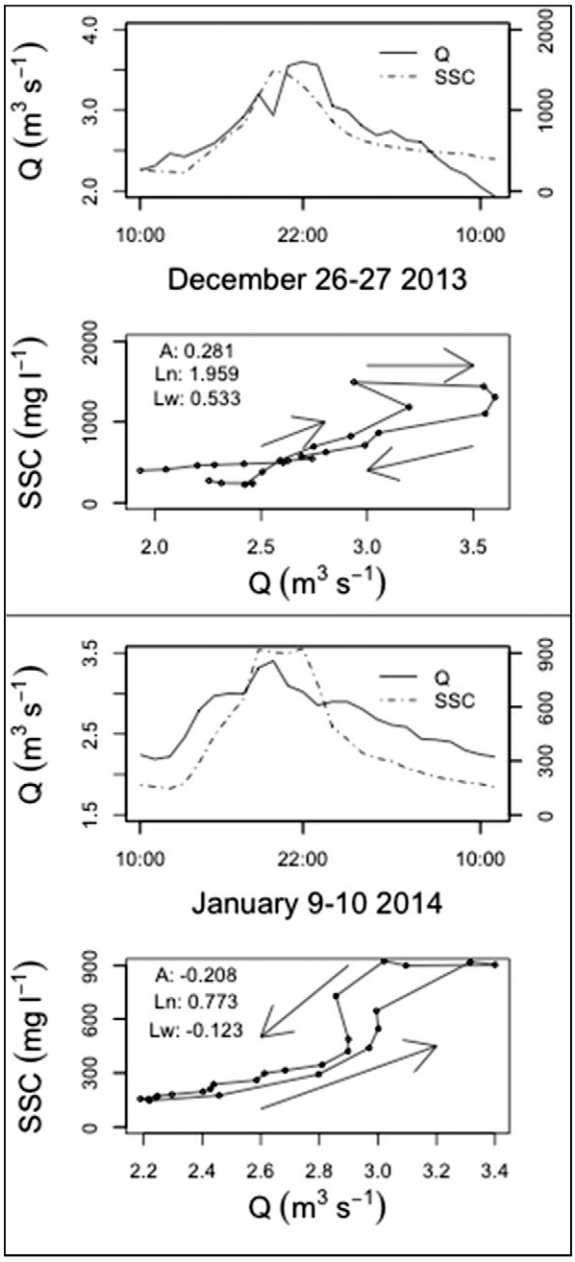

Fig. 6. Daily fluctuations of discharge and suspended sediment transport and hysteresis for two events occurred on the 26–27 December 2013 and 9–10 January 2014 as registered in the monitoring site D.

of Q and SSC are common on the registered series, the centre of mass of the daily fluctuations of Q and SSC was calculated and their lags between monitoring sites A and D were obtained. Fig. 8 shows the celerity of the center of mass of daily fluctuations of discharge and suspended sediment transport from A to D in terms of velocity. It appears that the propagation of the hydrograph is slower during late glacier melting (February and March) than during late snowmelt and early glacier melting (November and December). This is likely due to the fact that in late February and March the only source of runoff is the glacierized area in the upper part of the basin, and that flood waves are simply routed downstream, at a speed of approximately 1 m s^{-1}, which is reasonable considering the slope of the main channel (Fig. 9). Instead, in November and December there is a certain runoff contribution generated by snowmelt and groundwater in the middle and lower portion of the basin, thus anticipating the arrival of the flood wave, and celerity deceptively appears to be higher, up to 10 m s^{-1} (Fig. 9). It is worth noticing that the celerity of the sediment wave appears to be relatively consistent through the seasons, being only slightly higher in November. Indeed, Fig. 8 shows that, irrespective of the celerity of the flood wave, sediments are transferred from A to D at a celerity comparable to the flood waves during glacier melting (around 0.8 m s^{-1}). This would suggest that, apart from the snowmelt period, the main source of fine sediments is located above the monitoring site A, and specifically the pro- and peri-glacier area.

4. Discussions

4.1. Suspended sediment yield in a glacierized basin of the southern Andes

Calculations of suspended sediment yields from the Andean rivers of Chile are still not abundant in the literature. Pepin et al. (2010) used daily values of SSC and Q to calculate suspended sediment yields from a wide variety of Chilean rivers, showing that values range generally from 0 to 700 t $year^{-1}$ km^{-2}. In central Chile, suspended sediment yield is mainly produced in summer. In the proximity of the study basin, Pepin et al. (2010) estimated a yield of around 500 t $year^{-1}$ km^{-2} on basins with an area between 1600 and 4800 km^2. These values are significantly higher than other basins in central Chile due to the presence of glaciers and the reduced percentage of forest cover. The value of specific suspended sediment yield obtained in the present study is around 470 t $year^{-1}$ km^{-2}, which is quite high considering that it was produced during only 6 months. This value is comparable with that reported for other glaciers (e.g. 290 t $year^{-1}$ km^{-2}, Dunagiri Glacier, Srivastava et al., 2014; 300–1300 t $year^{-1}$ km^{-2}, Siachen Glacier, Bhutiyani, 2000). Yet, this value is one order of magnitude lower than what reported for other Himalayan and Alpine glaciers (e.g. 4800 t $year^{-1}$ km^{-2}, Gangotri Glacier, Haritashya et al., 2006; 4500 t $year^{-1}$ km^{-2}, Haut Glacier d'Arolla, Hodgkins et al., 1997).

In the Estero Morales, approximately half of the suspended sediment yield is due to snowmelt and half to glacier melting. This is due to the high elevation of the study basin and to the Mediterranean type of climate, which lead to the lack of considerable rainfall events in summertime. This makes the Estero Morales substantially different than other glacierized basins on other latitudes, where typically three periods of sediment yield could be depicted, namely snowmelt, glacier melt and rainfall events, and single rainfall events do not play an important role in activating sediment sources (e.g. Schiefer et al., 2006; Beylich and Kneisel, 2009; Beylich et al., 2010).

4.2. Dynamics of suspended sediment yield and availability in a glacierized basin

Data provided by the Estero Morales show that from early snowmelt to late glacier melting, there is a progressive reduction of suspended sediment concentration for a specific discharge, i.e. progressively higher discharges are needed to transport the same amount of sediments (in g l^{-1}). This is probably due to the reduced snow cover from the ablation area and the progressively limited amount of subglacial sediments. Because the upper part of the glacierized areas are not covered by as much debris as the lower portion of the glacier, it is likely that a textural study could shed light on the relative importance of glacier melting from the upper and lower part of the glacierized area. As showed by Haritashya et al. (2010) among others, the size of transported sediments can reveal the origin of sediments, which is likely to be subglacial from the upper part of the basin and supraglacial from the lower part of the debris-cover glacierized area.

The analysis of suspended sediment transport and hysteresis at the daily scale in the Estero Morales allows inference of the dynamics of sediment availability in a small glacierized basin. Fig. 10 shows a conceptual model that helps explain the dynamics of sediment availability and hysteresis in a glacierized basin such as the Estero Morales.

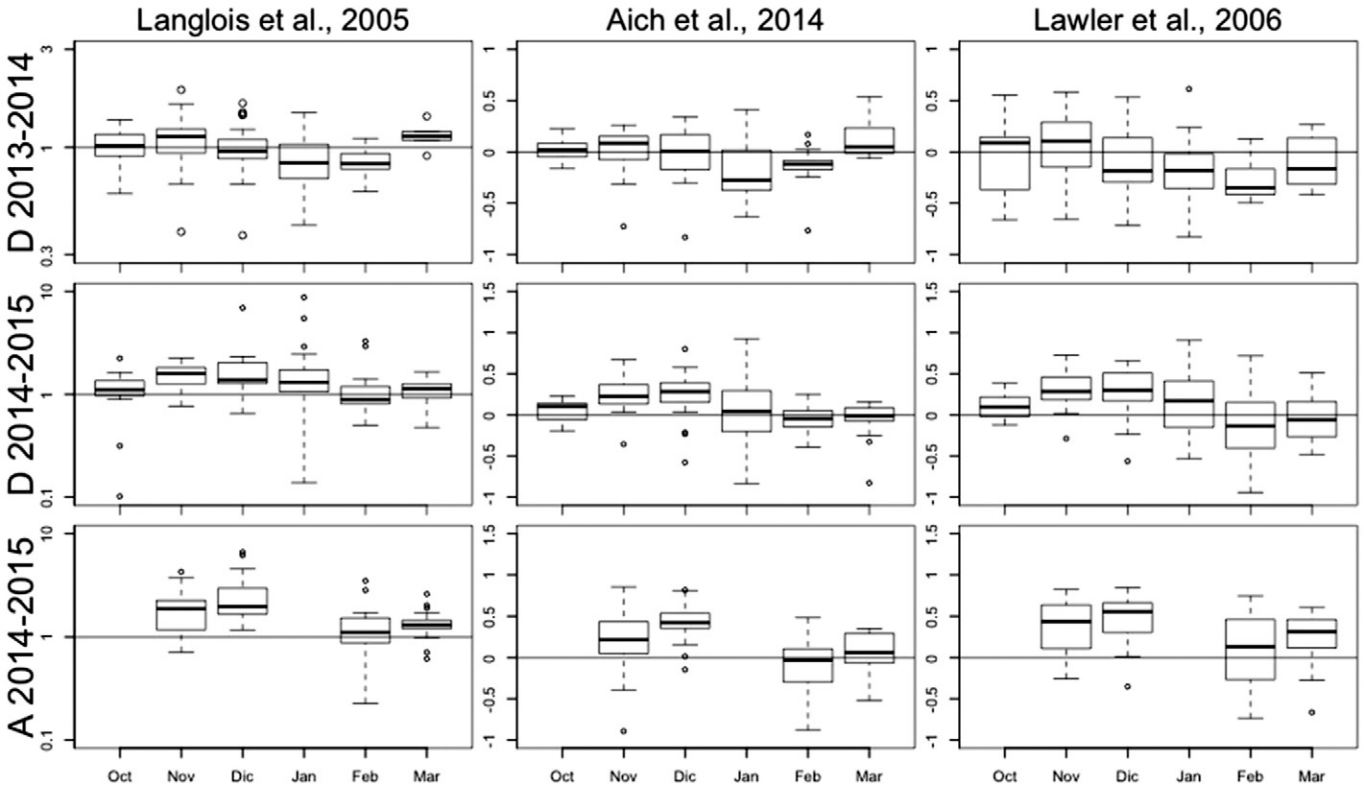

Fig. 7. Distribution of hysteresis magnitude as calculated using Langlois et al. (2005); Aich et al. (2014), and the Lawler et al. (2006) hysteresis indices on monitoring sites A and D on the monitoring seasons 2013–2014 and 2014–2015.

At the beginning of the snowmelt season the basin is almost completely covered by snow, and the sources of fine sediments for the first flood events are the slopes and the lower portion of the channel bed. Frozen soils usually limit water infiltration at spring melt, facilitating soil erosion and the delivery of fine sediments to the main stream. The stream channel itself can also represent a source of fine sediment due to bank erosion during the first events (e.g. Nolan and Hill, 1987) and the remobilization of fine sediments from the channel bed. Because sediment sources are ready-available and very close to the monitoring site, hysteresis patterns associated to single events tend to be very weak. However, even if moderate discharges can transport high concentration of suspended sediments (see Fig. 4), snowmelt floods are limited in number and magnitude, so that the overall suspended sediment yield is relatively low (see Fig. 5).

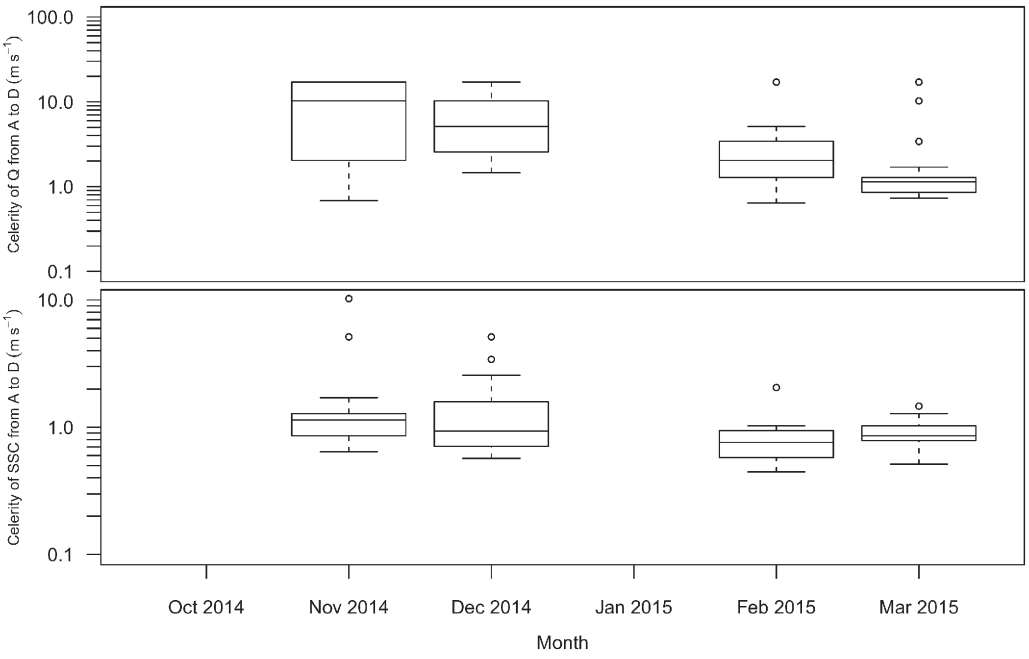

Fig. 8. Celerity of daily fluctuations of discharge (above) and suspended sediment waves (below) propagation from monitoring sites A and D.

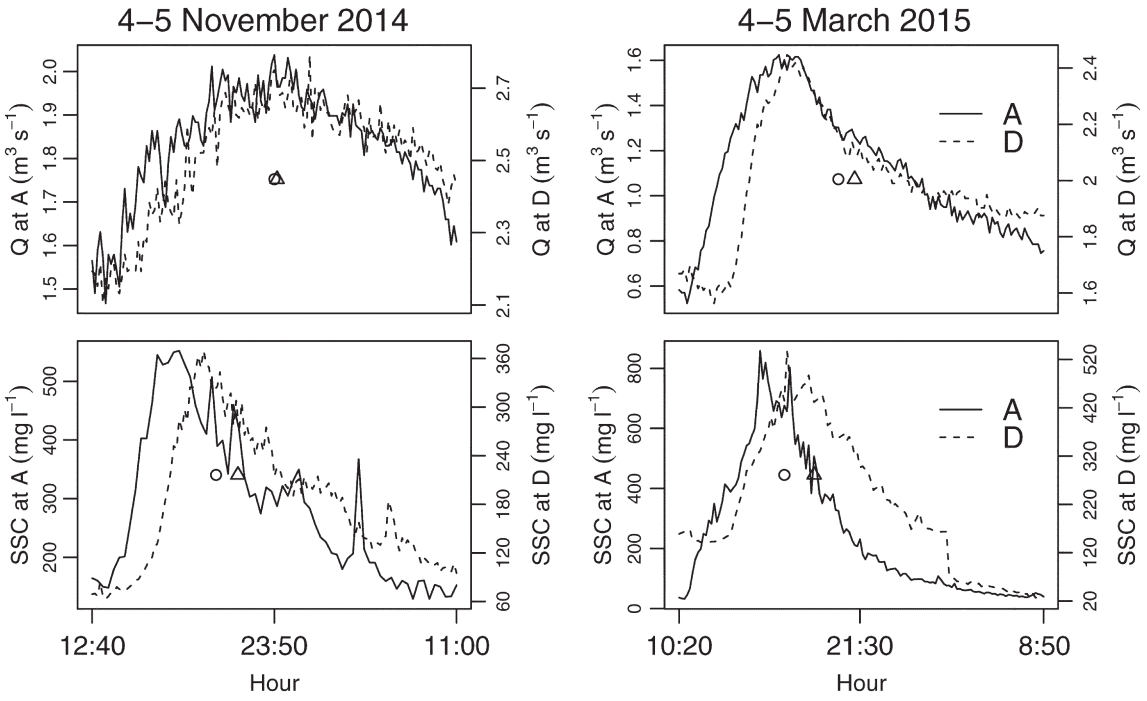

Fig. 9. Examples of daily changes of discharge (Q) and suspended sediment concentration (SSC) as measured in the monitoring sites A and D in November (on the left) and March (on the right). Center of masses of the curves are represented in triangular and circular icons for A and D, respectively. The celerity of the center of mass of discharge from A to D is approximately 10.2 and 1.7 m s^{-1} in November and March, respectively. The celerity of the center of mass of SSC from A to D is approximately 1.1 and 0.9 m s^{-1} in November and March, respectively.

Towards the middle of the snowmelt season (approximately November in the Estero Morales), the hillslopes of the middle part of the basin and the main channel keep furnishing fine sediments, but the proglacial areas starts to be active too, as the glacierized areas begins to melt. Sediment availability is still very high and relatively close to the monitoring point. Owing to the proximity of sediment sources (Asselman, 1999; Gao and Pasternack, 2007) and the probable dilution effect due to the greater contribution of subsurface water to stream flow during the recession stage of the hydrographs (Wood, 1977), the hysteresis loops of daily floods tend to be clockwise.

During the glacier melt season (approximately from December to February in the Estero Morales), the proglacial area is the main source of sediments transported in suspension by the daily floods. Sediment availability is high during the glacier melting season, which in fact contributes the most to the overall sediment yield from the Estero Morales. However, because the main sediment source is far from the monitoring

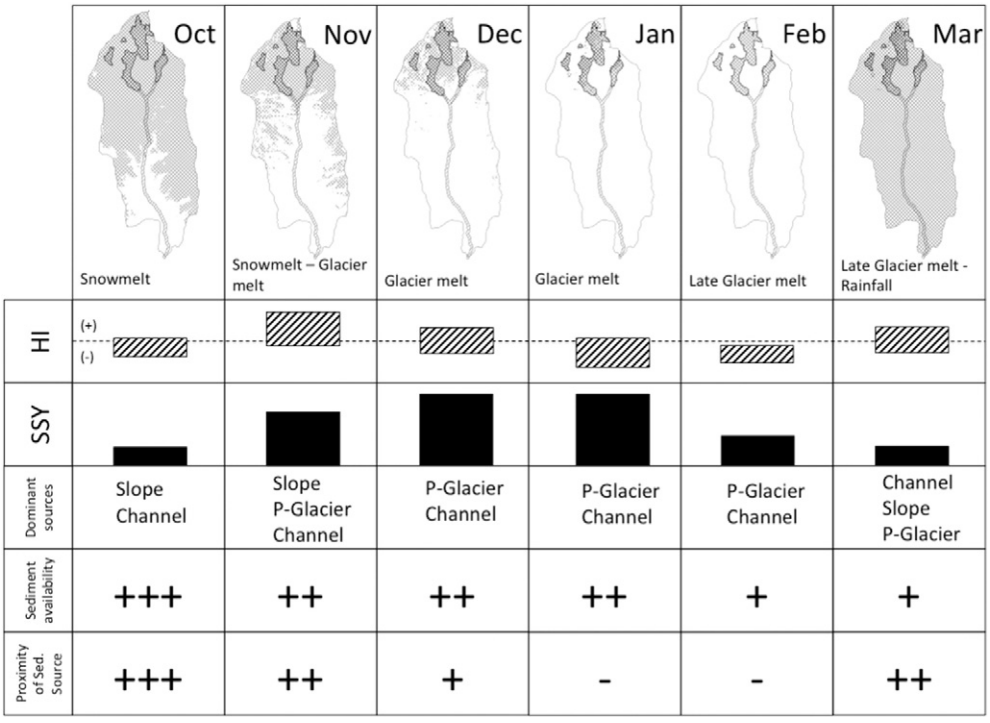

Fig. 10. Conceptual model of the spatial and temporal changes of sediment yield, sources, and predominant hysteresis patterns of daily fluctuations of discharge in the Estero Morales

site, the hysteresis pattern for daily floods tends to become counterclockwise. This is increasingly more evident towards the end of the glacier melt season, as the groundwater contribution to hydrographs reduces and fine sediment in the main channel becomes depleted. Regarding hysteresis during glacier melting floods, evidence from the literature is somehow contrasting. Singh et al. (2005) analysed hysteresis during melting of the Gangotri glacier in the Himalayas, reporting mostly clockwise hysteresis, whereas in other environments, counterclockwise hysteresis was more common (e.g. Lawler et al., 1992).

At the very end of the glacier melting season and before precipitation begins to fall as snow, the sediment yield is very limited due to the very low magnitude of daily floods and the progressive reduction of sediment availability from the proglacial area. This progressive reduction of suspended sediment concentration and yield towards the end of the melting season has been previously reported and related to limited sediment availability in the subglacial or morainic areas (Østrem, 1975; Collins, 1990; Haritashya et al., 2006). However, because of the first rainfall events that normally occur in this period, hysteresis patterns are not dominated anymore by counterclockwise loops, as during rainfall events the main sediment source is the whole basin and clockwise loops are featured.

Overall, the reduction of suspended sediment transport and tendency from clockwise to counterclockwise hysteresis from early snowmelt to late glacier melt in the Estero Morales has been explained here mainly in terms of depletion of sediments from the subglacial area and ablation front, as previously done in other environments (e.g. Gabet et al., 2008). However, Andermann et al. (2012) showed that groundwater dilution can also help to explain the fate of clockwise hysteresis in glacierized basins. Even if rainfall events are not common and their contribution to suspended sediment yield is negligible in the Estero Morales, it is possible that a progressive recharge of groundwater storage in the basin can be partially claimed to explain the increase of hydrograph celerity from monitoring site A to D during snowmelt (see Fig. 8) and the delay in the arrival of suspended sediments (producing counterclockwise hysteresis). To further explore this possibility, a series of water samples along the 2014–2015 season have been taken at monitoring sites A and D in order to analyse the content of stable isotope of water, which can substantially help in deciphering the main sources (groundwater vs. snowmelt vs. glacier melt) contributing to runoff (e.g. Cable et al., 2011; Penna et al., 2014).

It seems worth stressing here that hysteresis studies generally tend to overlook the fact that the direction and the magnitude of hysteretic patterns are inevitably related to the distance between the likely source of sediments and the monitoring point. Intuitively, the scatter of the relationship between discharge and suspended sediments would increase if the two variables are measured far from the source of runoff and sediments. In the Estero Morales, no significant differences are evident if hysteresis from monitoring points A and D is compared. This could be due to the fact that the basin is narrow, with a lack of significant tributaries from A to D that can add complexities to the conveyance of water and sediment waves from A to D, at least when the source of runoff is essentially the glacier (see Fig. 8). Also, the hysteresis pattern is generally already visible in monitoring site A, probably due to the fact that the glacierized area in the basin is topographically complex, being divided in several small glacier bodies (some covered by debris and some not), and spanning a wide range of elevations (Fig. 1). In order to shed light on this process of generation and transfer of the hysteretic patterns downstream, multiple monitoring sites would be required along the main channel, and field experience of similar investigations is still not available. Also, it seems worth stressing the importance of monitoring suspended sediment yield over long term scales, as sediment concentration can be very sensitive to snowfall (Iida et al., 2012), climate during the melting seasons (Beylich et al., 2010; Gao and Josefson, 2012), sediment sources at the basis scale (e.g. Mills and Bathurst, 2015), and high-magnitude events (e.g. Schiefer et al., 2010). Long term monitoring programs are needed in order to assess responses to glacier retreat in terms of sediment storage and yield.

5. Final remarks

This paper presents a temporal study of suspended sediment yield in a small glacierized basin in the Southern Chilean Andes. Relationships between suspended sediment concentration and discharge, and hysteretic patterns of daily fluctuations of discharge due to snow and glacier melting are used to infer temporal changes in sediment sources and availability as:

- early snowmelt: fine sediments are provided by the lower part of the basin where snow is melting; sediment availability is almost unlimited and high sediment concentrations are transported by relatively low discharges; hysteresis patterns are not very evident because sediment sources are readily-available and very close to the monitoring site;
- late snowmelt and early glacier melting: fine sediments are provided by the middle part of the basin, sediment availability is still very high and high sediment concentrations are transported by relatively low discharges; the main sources are relatively close to the monitoring site and hysteresis patterns tend to be clockwise as the peaks of suspended concentration anticipate the peak of discharges on daily hydrographs;
- glacier melting: fine sediments are provided by the proglacial area, far from the monitoring site, making the daily hydrographs feature counterclockwise hysteresis with suspended sediment concentration. Higher discharges are necessary to transport a certain concentration of sediments if compared with snowmelt. Because of the higher discharges the sediment yield due to glacier melting is very high; and
- late glacier melting: sediment availability from the proglacial area reduces progressively, and sediment sources at the basin scale are activated by rainfall events; hysteresis tends to be more counterclockwise if compared with the glacier melting season; sediment yield is very low.

Acknowledgments

The research was supported by the projects FONDECYT 1130378 and IDRC 107081-001. We are grateful to the Corporación Nacional Forestal (CONAF) for the interest and support in this study. We thank Joaquin Lobato, Juan Pablo del Pedregal, and Riccardo Rainato for their help in the field. Tim Stott and an anonymous reviewer are kindly thanked for their contributions that helped to improve an earlier version of this paper.

References

Aich, V., Zimmermann, A., Elsenbeer, H., 2014. Quantification and interpretation of suspended-sediment discharge hysteresis patterns: how much data do we need? Catena 122, 120–129. http://dx.doi.org/10.1016/j.catena.2014.06.020.

Andermann, C., Longuevergne, L., Bonnet, S., Crave, A., Davy, P., Gloaguen, R., 2012. Impact of transient groundwater storage on the discharge of Himalayan rivers. Nat. Geosci. 5, 127–132. http://dx.doi.org/10.1038/ngeo1356.

Asselman, N.E.M., 1999. Suspended sediment dynamics in a large drainage basin: the River Rhine. Hydrol. Process. 13, 1437–1450.

Beylich, A.A., Kneisel, C., 2009. Sediment budget and relief development in Hrafndalur, subarctic oceanic Eastern Iceland. Arct. Antarct. Alp. Res. 41, 3–17. http://dx.doi.org/10.1657/1523-0430-41.1.

Beylich, A.A., Liermann, S., Laute, K., 2010. Fluvial transport during thermally and pluvially induced peak runoff events in a glacier-fed mountain catchment in western Norway. Geogr. Ann. A92, 237–246. http://dx.doi.org/10.1111/j.1468-0459.2010.00392.x.

Bhutiyani, M.R., 2000. Sediment load characteristics of a proglacial stream of Siachen Glacier and the erosion rate in Nubra valley in the Karakoram Himalayas. India. J. Hydrol. 227, 84–92. http://dx.doi.org/10.1016/S0022-1694(99)00174-2.

Bilotta, G.S., Brazier, R.E., 2008. Understanding the influence of suspended solids on water quality and aquatic biota. Water Res. 42, 2849–2861. http://dx.doi.org/10.1016/j.watres.2008.03.018.

Blettler, M.C.M., Amsler, M.L., Ezcurra de Drago, I., Espinola, L., Eberle, E., Paira, A., Best, J.L., Parsons, D.R., Drago, E.E., 2015. The impact of significant input of fine sediment on benthic fauna at tributary junctions: a case study of the Bermejo-Paraguay River confluence, Argentina. Ecohydrology 8, 340–352. http://dx.doi.org/10.1002/eco.1511.

Cable, J., Ogle, K., Williams, D., 2011. Contribution of glacier meltwater to streamflow in the Wind River Range, Wyoming, inferred via a Bayesian mixing model applied to isotopic measurements. Hydrol. Process. 25, 2228–2236. http://dx.doi.org/10.1002/hyp.7982.

Collins, D.N., 1990. Seasonal and annual variations of suspended sediment transport in meltwaters draining from an Alpine glacier. Proceedings of Two Lausanne Symposium, IAHS Publ. no. 193 1990, pp. 439–446.

Collins, L., Zhang, Y.S., Hickinbotham, R., Bailey, G., Darlington, S., Grenfell, S.E., Evans, R., Blackwell, M., 2013. Contemporary fine-grained bed sediment sources across the River Wensum Demonstration Test Catchment, UK. Hydrol. Process. 27, 857–884. http://dx.doi.org/10.1002/hyp.9654.

Curran, J.C., Wilcock, P.R., 2005. Effect of sand supply on transport rates in a gravel-bed channel. J. Hydraul. Eng. 131, 961–967. http://dx.doi.org/10.1061/(ASCE)0733-9429(2005)131:11(961).

Davis, C.M., Fox, J.F., 2009. Sediment fingerprinting: review of the method and future improvements for allocating nonpoint source pollution. J. Environ. Eng. 135, 490–504. http://dx.doi.org/10.1061/(ASCE)0733-9372(2009)135:7(490).

Duvert, C., Gratiot, N., Evrard, O., Navratil, O., Némery, J., Prat, C., Esteves, M., 2010. Drivers of erosion and suspended sediment transport in three headwater catchments of the Mexican Central Highlands. Geomorphology 123, 243–256. http://dx.doi.org/10.1016/j.geomorph.2010.07.016.

Fan, X., Shi, C., Shao, W., Zhou, Y., 2013. The suspended sediment dynamics in the Inner-Mongolia reaches of the upper Yellow River. Catena 109, 72–82. http://dx.doi.org/10.1016/j.catena.2013.05.010.

Gabet, E.J., Burbank, D.W., Pratt-Sitaula, B., Putkonen, J., Bookhagen, B., 2008. Modern erosion rates in the High Himalayas of Nepal. Earth Planet. Sci. Lett. 267, 482–494. http://dx.doi.org/10.1016/j.epsl.2007.11.059.

Gao, P., Josefson, M., 2012. Event-based suspended sediment dynamics in a central New York watershed. Geomorphology 139–140, 425–437. http://dx.doi.org/10.1016/j.geomorph.2011.11.007.

Gao, P., Pasternack, G., 2007. Dynamics of suspended sediment transport at field-scale drain channels of irrigation-dominated watersheds in the Sonoran desert, southeastern California. Hydrol. Process. 21, 2081–2092. http://dx.doi.org/10.1002/hyp.6398.

Haddadchi, A., Ryder, D.S., Evrard, O., Olley, J., 2013. Sediment fingerprinting in fluvial systems: review of tracers, sediment sources and mixing models. Int. J. Sediment Res. 28, 560–578. http://dx.doi.org/10.1016/S1001-6279(14)60013-5.

Haritashya, U.K., Singh, P., Kumar, N., Gupta, R.P., 2006. Suspended sediment from the Gangotri Glacier: quantification, variability and associations with discharge and air temperature. J. Hydrol. 321, 116–130. http://dx.doi.org/10.1016/j.jhydrol.2005.07.037.

Haritashya, U.K., Kumar, A., Singh, P., 2010. Particle size characteristics of suspended sediment transported in meltwater from the Gangotri Glacier, central Himalaya - an indicator of subglacial sediment evacuation. Geomorphology 122, 140–152. http://dx.doi.org/10.1016/j.geomorph.2010.06.006.

Hodgkins, R., Tranter, M., Dowdeswell, J., 1997. Solute provenance, transport and denudation in a high Arctic glacierised catchment. Hydrol. Process. 11, 1813–1832.

Iida, T., Kajihara, A., Okubo, H., Okajima, K., 2012. Effect of seasonal snow cover on suspended sediment runoff in a mountainous catchment. J. Hydrol. 428–429, 116–128. http://dx.doi.org/10.1016/j.jhydrol.2012.01.029.

Infante Fabres, N.O., 2009. El monumento natural El Morado. Análisis del Medio Biofísico, Paisaje y Propuesta para Su gestión. Universitat de Barcelona, Spain.

Klein, M., 1984. Anti clockwise hysteresis in suspended sediment concentration during individual storms. Catena 11, 251–257. http://dx.doi.org/10.1016/S0341-8162(84)80024-7.

Langlois, J.L., Johnson, D.W., Mehuys, G.R., 2005. Suspended sediment dynamics associated with snowmelt runoff in a small mountain stream of Lake Tahoe (Nevada). Hydrol. Process. 19, 3569–3580. http://dx.doi.org/10.1002/hyp.5844.

Lawler, D.M., Dolan, M., Tomasson, H., Zophoniasson, S., 1992. Temporal variability of suspended sediment flux from a subarctic glacial river, southern Iceland. In: Bogen, J., Walling, D.E., Day, T.J. (Eds.), Erosion and Sediment Transport Monitoring Programmes in River Basins. IAHS Publication no. 210, Oslo, pp. 233–244.

Lawler, D.M., Petts, G.E., Foster, I.D.L., Harper, S., 2006. Turbidity dynamics during spring storm events in an urban headwater river system: the Upper Tame, West Midlands, UK. Sci. Total Environ. 360, 109–126. http://dx.doi.org/10.1016/j.scitotenv.2005.08.032.

Lenzi, M.A., Marchi, L., 2000. Suspended sediment load during floods in a small stream of the Dolomites (northeastern Italy). Catena 39, 267–282.

Martínez-Carreras, N., Krein, A., Gallart, F., Iffly, J.F., Pfister, L., Hoffmann, L., Owens, P.N., 2010. Assessment of different colour parameters for discriminating potential suspended sediment sources and provenance: a multi-scale study in Luxembourg. Geomorphology 118, 118–129. http://dx.doi.org/10.1016/j.geomorph.2009.12.013.

Masiokas, M.H., Rivera, A., Espizua, L.E., Villalba, R., Delgado, S., Aravena, J.C., 2009. Glacier fluctuations in extratropical South America during the past 1000 years. Palaeogeogr. Palaeoclimatol. Palaeoecol. 281, 242–268. http://dx.doi.org/10.1016/j.palaeo.2009.08.006.

Mills, C.F., Bathurst, J.C., 2015. Spatial variability of suspended sediment yield in a gravel-bed river across four orders of magnitude of catchment area. Catena 133, 14–24. http://dx.doi.org/10.1016/j.catena.2015.04.008.

Montgomery, D.R., Buffington, J.M., 1997. Channel-reach morphology in mountain drainage basins. Geol. Soc. Am. Bull. 109, 596–611.

Moore, R.D., 2005. Slug injection using salt in solution. Streamline Watershed Manag. 8, 1–6. http://dx.doi.org/10.1592/phco.23.9.1S.32890.

Motha, J.A., Wallbrink, P.J., Hairsine, P.B., Grayson, R.B., 2003. Determining the sources of suspended sediment in a forested catchment in southeastern Australia. Water Resour. Res. 39, 1056. http://dx.doi.org/10.1029/2001WR000794.

Nolan, K.M., Hill, B.R., 1987. Sediment budget and storm effects in a drainage basin tributary to Lake Tahoe. Eos 68, 305.

Østrem, G., 1975. Sediment transport in glacial melt water streams. In: Jopling, A.V., McDonald, B.C. (Eds.), Glaciofluvial and Glaciolacustrine Sedimentation, Society of Economic Paleontologists and Mineralogists. vol. 23, pp. 101–122 Special Publication.

Owens, P.N., Batalla, R.J., Collins, A.J., Gomez, B., Hicks, D.M., Horowitz, A.J., Kondolf, G.M., Marden, M., Page, M.J., Peacock, D.H., Petticrew, E.L., Salomons, W., Trustrum, N.A., 2005. Fine-grained sediment in river systems: environmental significance and management issues. River Res. Appl. 21, 693–717. http://dx.doi.org/10.1002/rra.878.

Pelliccioti, F., Ragettli, S., Carenzo, M., McPhee, J., 2014. Changes of glaciers in the Andes of Chile and priorities for future work. Sci. Total Environ. 493, 1197–1210. http://dx.doi.org/10.1016/j.scitotenv.2013.10.055.

Penna, D., Engel, M., Mao, L., Dell'Agnese, a., Bertoldi, G., Comiti, F., 2014. Tracer-based analysis of spatial and temporal variation of water sources in a glacierized catchment. Hydrol. Earth Syst. Sci. Discuss. 11, 4879–4924. http://dx.doi.org/10.5194/hessd-11-4879-2014.

Pepin, E., Carretier, S., Guyot, J.L., Escobar, F., 2010. Specific suspended sediment yields of the Andean rivers of Chile and their relationship to climate, slope and vegetation. Hydrol. Sci. J. 55, 1190–1205. http://dx.doi.org/10.1080/02626667.2010.512868.

Rinaldi, M., Casagli, N., Dapporto, S., Gargini, A., 2004. Monitoring and modelling of pore water pressure changes and riverbank stability during flow events. Earth Surf. Process. Landf. 29, 237–254. http://dx.doi.org/10.1002/esp.1042.

Rivera, A., Casassa, G., Acuña, C., Lange, H., 2000. Variaciones recientes de glaciares en Chile. Invest. Geogr. Chile 34, 29–60.

Rovira, A., Batalla, R.J., 2006. Temporal distribution of suspended sediment transport in a Mediterranean basin: The Lower Tordera (NE SPAIN). Geomorphology 79, 58–71. http://dx.doi.org/10.1016/j.geomorph.2005.09.016.

Ryan, P., 1991. Environmental effects of sediment on New Zealand streams: a review. N. Z. J. Mar. Freshw. Res. 25, 207–221. http://dx.doi.org/10.1080/00288330.1991.9516472.

Schiefer, E., Menounos, B., Slaymaker, O., 2006. Extreme sediment delivery events recorded in the contemporary sediment record of a montane lake, southern Coast Mountains, British Columbia. Can. J. Earth Sci. http://dx.doi.org/10.1139/e06-056.

Schiefer, E., Hassan, M., Menounos, B., Pelpola, C.P., Slaymaker, O., 2010. Interdecadal patterns of total sediment yield from a montane catchment, southern Coast Mountains, British Columbia, Canada. Geomorphology 118, 207–212. http://dx.doi.org/10.1016/j.geomorph.2010.01.001.

Singh, P., Haritashya, U.K., Ramasastri, K.S., Kumar, N., 2005. Diurnal variations in discharge and suspended sediment concentration, including runoff-delaying characteristics, of the Gangotri Glacier in the Garhwal Himalayas. Hydrol. Process. 19, 1445–1457. http://dx.doi.org/10.1002/hyp.5583.

Srivastava, D., Kumar, A., Verma, A., Swaroop, S., 2014. Characterization of suspended sediment in meltwater from Glaciers of Garhwal Himalaya. Hydrol. Process. 28, 969–979. http://dx.doi.org/10.1002/hyp.9631.

Stott, T., Nuttall, A.-M., Biggs, E., 2014. Observed run-off and suspended sediment dynamics from a minor glacierized basin in south-west Greenland. Geogr. Tidsskr. J. Geogr. 114, 1–16. http://dx.doi.org/10.1080/00167223.2013.862911.

Walling, D.E., Amos, C.M., 1999. Source, storage and mobilisation of fine sediment in a chalk stream system. Hydrol. Process. 13, 323–340. http://dx.doi.org/10.1002/(SICI)1099-1085(19990228)13:3<323::AID-HYP741>3.0.CO;2-K.

Walling, D.E., Webb, B.W., 1982. Sediment availability and the prediction of storm-period sediment yields. Recent Dev. Explan. Predict. Eros. Sediment Yield (Proceedings Exet. Symp.). 137, pp. 327–337.

Walling, D.E., Collins, A.L., Jones, P.A., Leeks, G.J.L., Old, G., 2006. Establishing fine-grained sediment budgets for the Pang and Lambourn LOCAR catchments, UK. J. Hydrol. 330, 126–141. http://dx.doi.org/10.1016/j.jhydrol.2006.04.015.

Wilber, D.H., Clarke, D.G., 2001. Biological effects of suspended sediments: a review of suspended sediment impacts on fish and shellfish with relation to dredging activities in estuaries. N. Am. J. Fish Manag. 21, 855–875. http://dx.doi.org/10.1577/1548-8675(2001)0212.0.CO.

Williams, G., 1989. Sediment concentration versus water discharge during single hydrologic events in rivers. J. Hydrol. 111, 89–106.

Wood, P.A., 1977. Controls of variation in suspended sediment concentration in the River Rother, West Sussex, England. Sedimentology 24, 437–445.

Wood, P.J., Armitage, P.D., 1999. Sediment deposition in a small lowland stream - management implications. Regul. Rivers Res. Manag. 15, 199–210.

Wulf, H., Bookhagen, B., Scherler, D., 2012. Climatic and geologic controls on suspended sediment flux in the Sutlej River Valley, western Himalaya. Hydrol. Earth Syst. Sci. 16, 2193–2217. http://dx.doi.org/10.5194/hess-16-2193-2012.

Yeshaneh, E., Eder, A., Blöschl, G., 2013. Temporal variation of suspended sediment transport in the Koga catchment, North Western Ethiopia and environmental implications. Hydrol. Process. 5984, 5972–5984. http://dx.doi.org/10.1002/hyp.10090.